Journal of
Mechanics of
Materials and Structures

SO... IS THIS A SURFACE-BREAKING CRACK?

Milan Poznic and Claudio Pecorari

Volume 1, Nº 4 April 2006

mathematical sciences publishers

JOURNAL OF MECHANICS OF MATERIALS AND STRUCTURES
Vol. 1, No. 4, 2006

SO... IS THIS A SURFACE-BREAKING CRACK?

MILAN POZNIC AND CLAUDIO PECORARI

An inspection technique used to assess the structural integrity of critical components in a nuclear power plant must be able to discern surface-breaking cracks from subsurface cracks. This work proposes an ultrasonic method to provide that information and presents a theoretical investigation into it. The main assumption of the model is that water carried by pressurized pipes infiltrates and fills a surface-breaking crack, while a subsurface crack is dry. The model simulates an inspection in which the modulation technique is employed and the surface hosting the crack is not accessible. A ratio, R, constructed with signals recorded in backscattering configuration during a modulation cycle, is examined and shown to provide a clear criterion allowing subsurface cracks to be distinguished from surface-breaking cracks when a shear vertical wave at 45 degree incidence is employed as a probe.

1. Introduction

Stress corrosion cracks, especially in pipes carrying pressurized water, constitute a serious threat to the structural integrity of nuclear power plants. They are often found in regions proximal to the inner surface of the pipe, and can be either surface-breaking or subsurface. The growth of a subsurface crack is caused mostly by fatigue. However, if a crack reaches the surface of the hosting component, corrosion becomes the main factor affecting crack growth. This is the case because water enters the fracture thanks to the combination of tensile stresses, which cause the crack to remain open while the plant is operating, and the pipe internal pressure, which can reach values of the order of 70 atm.

For this reason, it is of the utmost importance for a nondestructive technique employed in the assessment of a plant's structural integrity to enable not only the detection of stress-corrosion cracks, but also their characterization as surface-breaking or subsurface defects. Indeed, there have been instances in which cracks have been characterized as subsurface during inspection but proved to be surface-breaking upon a destructive metallurgical investigation [Jenssen et al. 2000]. Of relevance to the subject of this work is also the presence of debris resulting from

Keywords: partially closed cracks, modulation, wave scattering stress-corrosion.

corrosion, which tends to bridge the gap between the surfaces, rendering the defect more transparent to an inspecting ultrasonic beam.

This work presents the principles of an ultrasound-based technique designed to discern partially closed cracks that are subsurface from those that are surface-breaking. The proposed method exploits the effects of water confinement within a partially closed, surface-breaking crack on the acoustic response of the defect. The sensitivity of the proposed technique to the presence of fluid trapped between the crack faces, and to compressive stresses acting on the crack, is examined. The emphasis on cracks that are partially closed derives from the near certainty that, following the shut-down of the plant prior to inspection, stresses due to the plant's operating conditions are removed and cracks tend to partially close, at least in vicinity of their tips (see [Newman et al. 2003], for example). This investigation is limited to the worst-case scenario in which the surface hosting the crack is not accessible and the inspection must be carried out from the outer surface of the component.

The article is organized as follows. We first report experimental results which illustrate the characteristic dependence of the stiffness on the pressure applied to dry and fluid-filled interfaces. We then present a model which evaluates the backscattering by partially closed, surface-breaking and subsurface cracks. To simulate the effect of partial closure on backscattering, spring boundary conditions are employed. Experimental results obtained on partially closed interfaces are employed in the theoretical model to describe the effect of water trapped within a surface-breaking fracture. The model is used to simulate experiments in which the partial closure of the crack is modulated by a low-frequency, high-amplitude wave while a probing ultrasonic wave interrogates the defect. We close with a discussion of the significance of these findings for the development of a method allowing water-confining, surface-breaking cracks and dry subsurface cracks to be distinguished from each other.

2. Dry and water-confining interfaces

The interaction between ultrasonic waves and interfaces formed by two rough, nonconforming surfaces in contact under increasing pressure has been investigated extensively both experimentally and theoretically; see for example [Baltazar et al. 2002; Baik and Thompson 1984; Drinkwater et al. 1996; Lavrentyev and Rokhlin 1998; Kim et al. 2004a]. Models have been developed that derive the macroscopic mechanical properties of such interfaces from those of the asperities in contact and from the topographical properties of the surfaces. This considerable effort notwithstanding, several of the outstanding issues concerning this problem still await a solution [Pecorari and Poznic 2006]. In particular, the effect of water

confined between surfaces in partial contact appears not to be accounted for by any available model.

In this section we present experimental results on both dry and water-confining interfaces and use them in the theoretical modeling of ultrasonic wave scattering by surface-breaking and subsurface cracks. The experimental set-up employed in this investigation is discussed in [Pecorari and Poznic 2006] and is not repeated here. The only noteworthy differences from our earlier experimental conditions are:

i. The nominal frequency of the transducer used to generate and receive the waves reflected by the imperfect interface is 2.25 MHz here.

ii. The measurements were carried out also with shear waves.

iii. The rms roughness of the two surfaces employed here was evaluated to be of the order of 0.2 μm. In all the measurements, the inspecting waves insonify the interface at normal incidence.

Among the properties of interest, the stiffness K of the imperfect interface is of primary importance in understanding the interaction between ultrasonic waves and such interfaces. It is defined by the relation $K = \partial P/\partial\delta$, where P is the applied pressure (or the tangential stress) and δ is the relative approach (or the tangential displacement) between the mean planes of the rough surfaces. The values K_N and K_T of the normal and transverse interfacial stiffness can be recovered from the measured reflection coefficients R_L and R_T for longitudinal and shear waves at normal incidence via the well-known relation

$$R_{L,T} = -\frac{1}{1 - 2j\,(K_{N,T}/\omega Z_{L,T})},$$

where ω is the circular frequency of the incident and scattered waves, and Z_L, Z_T are the acoustic longitudinal and shear impedances of the medium. The symbol j represents the imaginary unit. When water is confined by the interface, and the real area over which mechanical contact between the surfaces take place is a small fraction of the nominal area, the normal stiffness of the latter can be written as the sum of two terms: $K_N = (\Lambda/d_0) + \Delta K_N$. The first term describes the effect of a layer of water with thickness d_0, the latter quantity being the distance between the mean planes of the rough surfaces when no pressure is applied to the interface. The symbol Λ represents the only nonzero elastic constant of the liquid medium. The second term, ΔK_N, describes the part of the stiffness which depends on the applied pressure. Since the shear modulus of water is zero, the transverse stiffness does not contain a term analogous to Λ/d_0.

Figure 1 reports experimental results obtained at normal incidence using steel-steel interfaces with rms roughness σ approximately equal to 0.2 microns. They

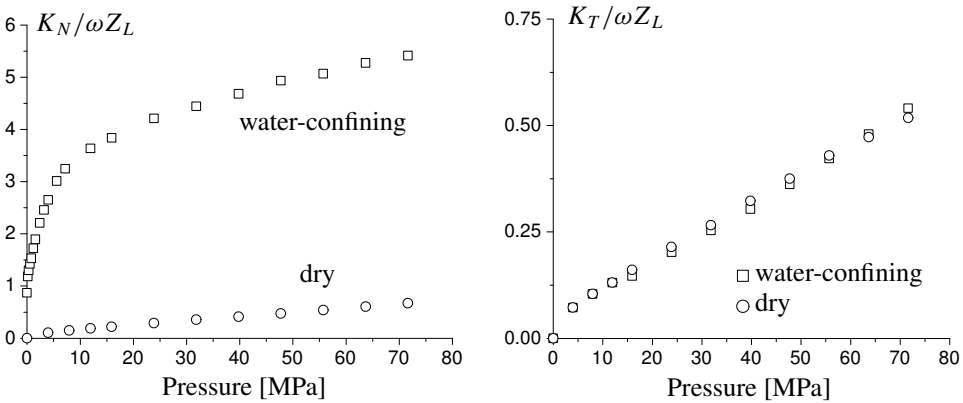

Figure 1. Normalized normal (left) and transverse (right) spring stiffness versus pressure applied to a water-confining and dry steel-steel interface. The symbols represent experimental results.

illustrate the dependence of the normalized normal, $K_N/\omega Z_L$, and transverse, $K_T/\omega Z_L$, interface stiffness components on the applied pressure for both dry and water-confining interfaces, respectively. The pressure is varied from 0 MPa to 80 MPa at which point the reflection coefficient of a longitudinal wave interacting with a water-confining interface is smaller than 0.1. The two most relevant features of Figure 1, left, are the overall larger normal stiffness of the water-confining interface compared to that of the dry one, and the initial fast increase of K_N when pressure not exceeding 5 MPa is applied to the interface. Unpublished numerical simulations by these authors show that the addition of the term accounting for the thin fluid layer, Λ/d, to the stiffness of the dry interface is not sufficient to reproduce the experimental results. A possible explanation for this deficiency of the model may be found in the results of both experimental and theoretical investigations into the interaction between solid surfaces confining water; see [Das et al. 1996; Israelachvili 1992; Grabbe and Horn 1993; Ho et al. 1998; Pashley and Israelachvili 1984]. These works show that repulsive forces between solid surfaces arise when the distance between the latter is comparable to the dimension of the fluid's molecules. The physical origin of such repulsive forces may vary from system to system, but common to all is the increase of structural order caused by the spatial confinement on the molecules of the fluid. These findings suggest that these repulsive forces may also occur between asperities of the system under investigation, opposing their mechanical contact when they are separated by a distance of the order of a nanometer. An alternative interpretation to that just outlined considers the effect of drainage forces which oppose the motion of the solid surfaces in the direction normal to their mean planes. A suitable mathematical model for such a phenomenon should extend the analysis carried out by Chan and Horn [1985] on

cylindrical surfaces with axes oriented normally to each other and to the direction of motion. Essential for the accuracy of the novel model, the extension of Chang and Horn's model should account for the statistical character of the surface profiles. Of importance is also the results concerning the shear stiffness, K_T, which have been obtained with the same two interfaces; see Figure 1, right. They display a dependence on the applied pressure which, for our purposes, can be assumed to be identical. In other words, they show that the viscosity of the fluid does not affect K_T, and thus, a mechanism which does not call upon the viscosity of the fluid appears to offer a more plausible explanation of the experimental observation. In summary, the experimental results of Figure 1 show that water strongly affects the dependence of the interface normal stiffness on the applied pressure, while it does not alter that of the shear stiffness.

3. Theory

Figure 2 illustrates the geometry of the material system and of the defect under consideration. The segment of material of length a separating the crack from the surface in the diagram on the left is also known as the *ligament*. With reference to Figure 2, and following the method developed by Achenbach et al. [1980] and Mendelsohn et al. [1980], the original problem posed by the scattering of an incident bulk wave onto the crack is decomposed into a symmetrical and an antisymmetrical part.

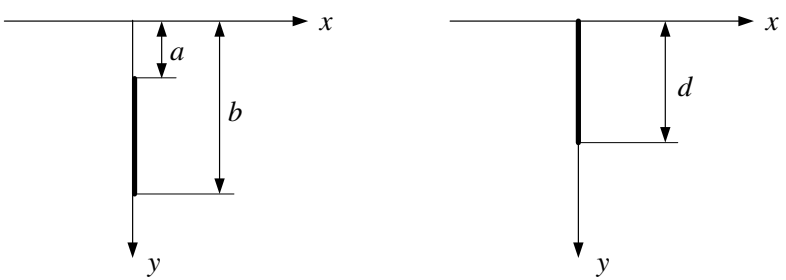

Figure 2. Geometry of the material system and its defect. The material system occupies the half-space $y > 0$. Left: Subsurface crack. Right: surface-breaking crack, with $a = 0$ and $b = d$.

When considering the scattering by a subsurface crack, the boundary conditions along the crack face, which are associated with the symmetrical problem are

$$\left.\begin{aligned} \sigma_{xy}^{+} &= 0, & x &= 0,\ \ 0 \le y < \infty, \\ \sigma_{xx}^{+} &= K_N\, \Delta u, & a &\le y < b, \\ u &= 0, & 0 &\le y < a \ \text{ or } \ b \le y < \infty, \end{aligned}\right\} \tag{3–1}$$

and those associated with the antisymmetrical problem are

$$\left.\begin{aligned} \sigma_{xx}^{+} &= 0, & x &= 0,\ \ 0 \le y < \infty, \\ \sigma_{xy}^{+} &= K_T \Delta v, & a &\le y < b, \\ v &= 0, & 0 &\le y < a \ \text{ or } \ b \le y < \infty. \end{aligned}\right\} \tag{3–2}$$

In these equations, the σ_{ii}^{+} are the total stress components acting on the positive side of the crack, i.e., on the side for which $x = 0^{+}$, while u and v are the displacement components in the x and y direction, respectively. The spring stiffness densities K_N and K_T are generally allowed to be functions of depth, y, so that nonuniform closure can be modeled. The remaining boundary conditions are those used by Achenbach et al. [1980] and Mendelsohn et al. [1980] for an open crack. In particular, the surface $y = 0$ is assumed to be free of traction. The crack closure is simulated by varying the contact pressure between the crack faces according to the next equations, which are given next only for a subsurface crack:

$$\begin{aligned} P(y) &= P_{\text{tip}} \exp \frac{y-b}{\ell}, & (a+b)/2 \le y \le b, \\ P(y) &= P_{\text{tip}} \exp \frac{a-y}{\ell}, & a \le y \le (a+b)/2. \end{aligned} \tag{3–3}$$

Here P_{tip} is the pressure at the crack tips and ℓ is the decay length which controls the spatial extent of the tip closure. The pressure distribution on a surface-breaking crack is obtained from (3–3) by letting $a = 0$ and substituting $(a+b)/2$ with $b = d$. Equations (3–3) are used to assign a local value to the spring stiffness densities by way of the relationships illustrated in Figure 1. The purpose of this feature of the model is twofold. First, the effect of the water on the scattering phenomenon is accounted for within the same mathematical scheme used to treat a dry partially closed crack. Secondly, the boundary conditions in equations (3–1) and (3–2) allow for the simulation of the well documented closure of a crack in the regions proximal to its tips [Newman et al. 2003], the causes of which are varied, still debated, and leading essentially to the same result when considered from the wave scattering point of view.

The equations of motion for the two displacement components are

$$c_L^2 \frac{\partial^2 u}{\partial x^2} + c_T^2 \frac{\partial^2 u}{\partial y^2} + \left(c_L^2 - c_T^2\right) \frac{\partial^2 v}{\partial x \partial y} = \frac{\partial^2 u}{\partial t^2},$$
$$c_L^2 \frac{\partial^2 v}{\partial x^2} + c_T^2 \frac{\partial^2 v}{\partial y^2} + \left(c_L^2 - c_T^2\right) \frac{\partial^2 u}{\partial x \partial y} = \frac{\partial^2 v}{\partial t^2},$$

where t represents time, and c_L and c_T are the phase velocities of longitudinal and shear waves, respectively. The solutions of these are given by the following expressions (see [Achenbach et al. 1980; Mendelsohn et al. 1980]):

$$u^s(\vec{x}) = \frac{2}{\pi} \int_0^\infty \left(\xi k_L A^s e^{-\alpha_L y} - 2\kappa^{-2} \alpha_T k_L C^s e^{-\alpha_T y}\right) \sin(\xi x)\, d\xi + \frac{2}{\pi} \int_0^\infty \left(\alpha_L k_L B^s e^{-\alpha_L x} + 2\kappa^{-2} \xi k_L D^s e^{-\alpha_T x}\right) \cos(\xi y)\, d\xi, \quad (3\text{–}4)$$

$$v^s(\vec{x}) = \frac{2}{\pi} \int_0^\infty \left(\alpha_L k_L A^s e^{-\alpha_L y} - 2\kappa^{-2} \xi k_L C^s e^{-\alpha_T y}\right) \cos(\xi x)\, d\xi + \frac{2}{\pi} \int_0^\infty \left(\xi k_L B^s e^{-\alpha_L x} + 2\kappa^{-2} \alpha_T k_L D^s e^{-\alpha_T x}\right) \sin(\xi y)\, d\xi, \quad (3\text{–}5)$$

for the symmetric field, while those of the antisymmetric are

$$u^a(\vec{x}) = \frac{2}{\pi} \int_0^\infty \left(\xi k_L A^a e^{-\alpha_L y} - 2\kappa^{-2} \alpha_T k_L C^a e^{-\alpha_T y}\right) \cos(\xi x)\, d\xi + \frac{2}{\pi} \int_0^\infty \left(\alpha_L k_L B^a e^{-\alpha_L x} + 2\kappa^{-2} \xi k_L D^a e^{-\alpha_T x}\right) \sin(\xi y)\, d\xi, \quad (3\text{–}6)$$

$$v^a(\vec{x}) = \frac{2}{\pi} \int_0^\infty \left(-\alpha_L k_L A^a e^{-\alpha_L y} + 2\kappa^{-2} \xi k_L C^a e^{-\alpha_T y}\right) \sin(\xi x)\, d\xi - \frac{2}{\pi} \int_0^\infty \left(\xi k_L B^a e^{-\alpha_L x} + 2\kappa^{-2} \alpha_T k_L D^a e^{-\alpha_T x}\right) \cos(\xi y)\, d\xi. \quad (3\text{–}7)$$

The time-dependence of the solution is assumed to be harmonic. In the equations above, $A^{a,s}$, $B^{a,s}$, $C^{a,s}$, and $D^{a,s}$ are functions of the integration variable ξ, and are themselves given in terms of integrals of suitable functions containing the tangential slope of the two components of the crack opening displacement. These are obtained by solving two decoupled singular integral equations derived by enforcing the boundary conditions (3–1) and (3–2) on the solutions of the equations of motion. The symbols k_L and k_T are the wavenumbers of the longitudinal and shear waves, respectively. With the same meaning of the subscripts L and T, the quantities α_L

and α_T are defined by

$$\alpha_L = \begin{cases} \sqrt{\xi^2 - k_L^2} & \text{if } \xi \geq k_L, \\ -j\sqrt{k_L^2 - \xi^2} & \text{if } \xi < k_L, \end{cases} \qquad \alpha_T = \begin{cases} \sqrt{\xi^2 - k_T^2} & \text{if } \xi \geq k_T, \\ -j\sqrt{k_T^2 - \xi^2} & \text{if } \xi < k_T. \end{cases}$$

The branch of the square root function in the complex plane is chosen to satisfy the Sommerfeld radiation condition.

Equations (3–4)–(3–7) concern the field in the quarter-space where both x and y are positive. The field components in the quarter-space where $x < 0$ are obtained from those given by those equations as follows:

$$u^s(x < 0, y) = -u^s(|x|, y), \qquad u^a(x < 0, y) = u^a(|x|, y),$$
$$v^s(x < 0, y) = v^s(|x|, y), \qquad v^a(x < 0, y) = -v^a(|x|, y).$$

In solving the integral equations in the unknown tangential slope of two components of the displacement discontinuity, the condition that their integral over the extent of the crack is null must be enforced. The scattering by an open subsurface crack was solved first by Brind and Achenbach [1981].

The scattering from a partially closed, surface-breaking crack is modeled within the same mathematical framework. The boundary conditions for this problem are obvious extensions of those given for a subsurface crack, and the solutions of the problem are again sought in the form given by equations (3–4)–(3–7).

As described earlier, the real physical system hosting the crack is a steel pipe containing water. Therefore, the boundary conditions stating that the surface $y = 0$ is traction-free are not correct. Enforcing the continuity of traction and normal displacement across the solid-water interface, however, would add considerable mathematical complications without substantially affecting the phenomena of interest in this work. In fact, the algorithm later proposed to characterize the defect as being surface-breaking or internal is designed to measure only the *relative* effect of the applied modulation on the scattering properties of the defect with respect to those displayed by the defect in its unperturbed state. Boundary conditions which amount to a small perturbation of the total field within the solid half-space are not expected to have a significant effect on the results of this algorithm.

4. Numerical results

The experimental results of Section 2 indicate that the most striking difference between the properties of two interfaces under consideration is the rapid increase of the normal stiffness of the water-confining interface as soon as contact between asperities is established. This naturally suggests the use of the parametric modulation technique as a novel method to characterize a crack as being surface-breaking or subsurface. The modulation technique exploits the nonlinear properties of partially

closed cracks, and more specifically the dependence of the crack stiffness on the applied pressure. Xiao and Nagy [1998] employed thermal stresses induced by a laser source to vary the closure of a surface-breaking crack which was simultaneously insonified by a high frequency Rayleigh wave. By means of suitable signal processing of the backscattered ultrasonic pulse acquired during different phases of the thermal modulation, these authors showed that the acoustic signature of the crack can be extracted from the noisy environment (see also [Nagy 1992]). In other words, the modulation technique was shown to be able to selectively detect nonlinear material defects. Rokhlin et al. [2004] adapted this method to increase the sensitivity of ultrasonic inspections to poor adhesive bonds between aluminum plates, while Kim et al. [2004b] (see also references therein) used it to characterize small surface-breaking cracks initiated at surface pits by fatigue. Finally, Kazakov et al. [2002] used the same idea to image the nonlinear properties of a surface-breaking crack. Rokhlin et al. [2004], Kim et al. [2004a; 2004b] and Kazakov et al. [2002] used a low-frequency source of mechanical vibrations to vary the instantaneous properties of the defect of interest.

In this work, an experimental configuration similar to those employed by the previously cited authors is simulated. A crack under investigation is subjected to a sinusoidal, time-dependent pressure field of amplitude ΔP: $P(t) = \Delta P \sin(\Omega t)$, the frequency of the modulation, Ω, being orders of magnitude lower than that of an ultrasonic wave, ω, which is used to monitor the instantaneous state of the crack. This pressure is superposed on the static pressure given in (3–3), which is responsible for the initial partial closure. During a cycle, three backscattered ultrasonic signals are recorded, two at the opposite turning points of each cycle, and one at the mid point when $P(t) = 0$. By using the peak-to-peak amplitude of the back-scattered wave, or any other feature of this signal which reflects the variation of the crack state, the following ratio is constructed:

$$R = \left(B^- - B^+\right)/B_0, \tag{4–1}$$

where $B^{-,+}$ are the features of interest measured when the crack is most open $(-)$ or closed $(+)$, respectively, and B_0 refers to the crack state in its rest condition. Note that the ratio R is independent of the amplitude of the incident wave, and, thus conveys information which depends on the intrinsic properties of the defect and of the modulation, but not on the intensity of the inspecting wave. This work investigates the conditions under which R can possibly serve as an "index of state" to distinguish a fluid filled surface-breaking crack from a dry subsurface crack. The numerical results presented next and the conclusions drawn from them refer to phenomena involving only monochromatic waves. However, given the linearity of the system, their validity can be extended to wave packets formed by linear superposition of harmonic waves.

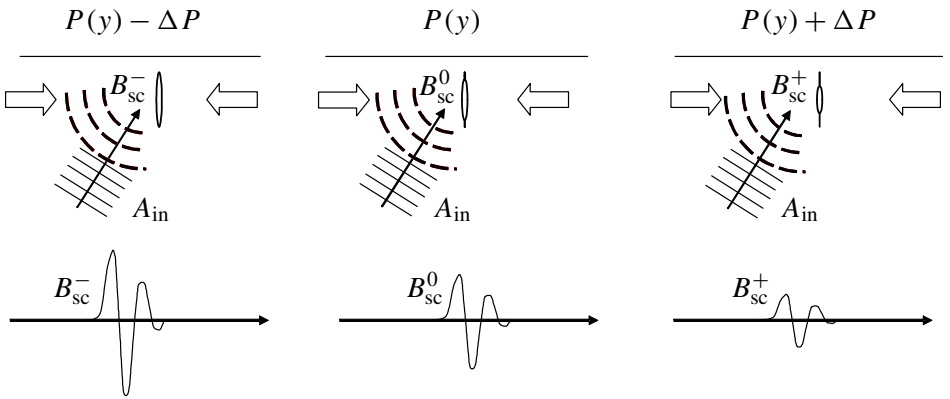

Figure 3. Schematics of the simulated modulation experiment illustrating the relationship between the state of the crack and the signal backscattered by it during a cycle of the modulation. The arrows pointing towards the crack represent the sum of the static pressure and the modulation.

The following numerical investigation considers the scattering by partially closed surface-breaking and subsurface cracks in a steel half-space. The mass density and phase velocity of longitudinal and shear waves in steel are $\rho = 7.8 \times 10^3\,\mathrm{kg\,m^{-3}}$, $c_L = 5900\,\mathrm{ms^{-1}}$, and $c_T = 3200\,\mathrm{ms^{-1}}$. The results presented in all the following figures refer to a configuration in which a shear vertical wave impinges on the defect at 45 degree incidence, unless otherwise stated. The frequency of the wave is $f = 2.25\,\mathrm{MHz}$. The solution of the scattering problem is evaluated in the backscattering direction. The observation point lies at a distance of about 30 shear wavelengths (about 40 mm) from the surface of the half-space.

The residual pressure which determines the closure of the crack (see Equation (3–3)) is chosen to represent three characteristic configurations: one in which the closure is uniform, and two in which it decays with rates equal to 0.1 mm and 1 mm, respectively. The rationale behind the choice of the latter values stems from the assumption that the cracks of interest are detectable by conventional methods, and, thus, their extent is of the order of several millimeters. For such cracks a likely state is one in which their tip(s) are partially closed while throughout the remaining portion of their extent there is no mechanical contact between the surfaces. The pressure at the crack tip, P_{tip}, is chosen to be equal to 5 MPa and 70 MPa to represent two well distinct situations in which the crack tip is nearly open or fairly closed, respectively. The values of the normalized stiffness constants $K_N/(\omega Z_L)$ and $K_T/(\omega Z_L)$ corresponding to these pressure values are 0.2 and 0.07, respectively, if the crack is dry, and 3 and 0.07 if a defect contains water. The amplitude

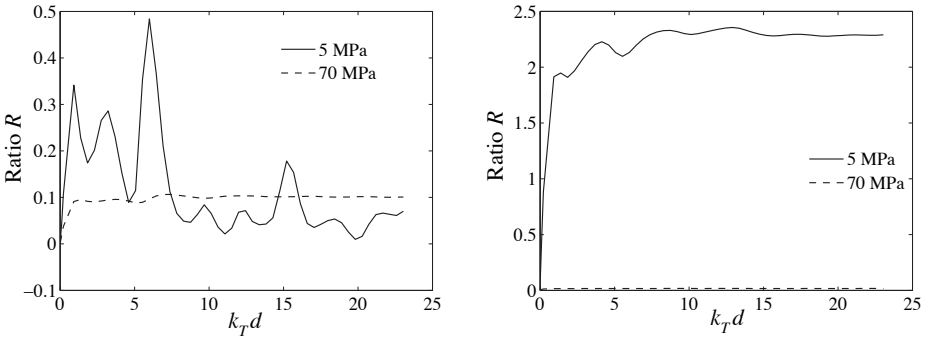

Figure 4. Ratio R versus nondimensional crack size $k_T d$ for values of pressure at the crack tip equal to 5 MPa and 70 MPa. The pressure distribution is constant along the crack extent. Left: dry surface-breaking crack. Right: water-confining surface-breaking crack.

of the modulation is $\Delta P = 5$ MPa in all simulations. For this value of the amplitude ΔP, the modulation causes the crack to open completely when $P_{\text{tip}} = 5$ MPa. The dependence of the ratio R on the nondimensional size of the crack, $k_T d$, is reported over a range which corresponds to cracks with physical dimension reaching values up to 5.36 mm.

In Figure 4, the left panel refers to a dry surface-breaking crack and the right panel to the same crack when it is filled with water. In both figures, the cases in which the crack is subjected to a uniform pressure, P_{tip}, of 5 MPa and 70 MPa are considered. In Figure 4, left, the crack shows a nearly constant response when $P_{\text{tip}} = 70$ MPa, reflecting the modest effect the modulation has on the crack opening, while it displays wide oscillation for the lower value of the applied pressure. In both cases, however, the ratio R does not exceeds values of 0.1 as the size of the crack increases. If water is confined within the crack (Figure 4, right), the value of the ratio for $P_{\text{tip}} = 70$ MPa is even smaller as a consequence of the higher values of the crack stiffness, while for $P_{\text{tip}} = 5$ MPa R reaches values larger than 2 over nearly all the range of values of $k_T d$ considered here. As indicated in Figure 2, right, the depth of the surface-breaking crack is d. This striking contrast is due to the large variation of values spanned by the normal stiffness as the total applied pressure varies between 0 and 10 MPa (see Figure 1, right).

Figure 5 illustrates the dependence of the ratio R for a surface-breaking crack with a closure given by the second equation of (3–3), specified for the case of a surface-breaking crack ($a = 0$, and $b = d$ as upper limit), and with $\ell = 1$ mm. As in the case considered in Figure 4, left, the response of a dry surface-breaking crack

tends to settle around values of the order of 0.1 as the size of the crack increases. However, a water-confining crack subjected to a compressive stress of 70 MPa at its crack tip (Figure 5, right) displays a remarkably different behavior compared to that shown in the corresponding panel of Figure 4. In fact, as the crack size exceeds the decay length, ℓ, corresponding to a value $k_T \ell \approx 5$, the ratio rapidly increases to reach values larger than one. This prediction can be explained as the result of an increasingly larger portion of the crack surface being subjected to a static pressure smaller than the amplitude of the modulation. Since the ratio R measures the relative variation of the backscattered signal caused by the modulation, the larger the portion of the crack, the opening of which is significantly affected by the modulation, the larger R. The extreme example of this situation is provided by the results of the previous figure in which ℓ is infinity. For $P_{\text{tip}} = 70$ MPa, the variation of the opening of the crack produces nearly no modulation of the scattered field since nowhere along the surface the crack opens. On the other hand, for $P_{\text{tip}} = 5$ MPa, the whole surface of the crack completely opens and closes, causing the largest variation of the backscattering considered in this work. The behavior of the curve associated with a pressure of 5 MPa at the crack tip may also be interpreted along the same line. Of interest is also the observation that the two curves appear to converge towards each other as the size of the crack increases. This result is further confirmed by those obtained if the decay length is decreased to become $\ell = 0.1$ mm, as shown in Figure 6, right. On the other hand, the predictions concerning a dry surface-breaking crack, which is partially closed by the same pressure field (Figure 6, left), do not present features which significantly differ from those already shown in the left panels of Figures 4 and 5. Also worthy of attention is the difference between the values of the plateau in the right panels of 5 and 6, the former being slightly larger than the latter (1 versus 0.75). This finding may be expected in virtue of positive correlation between the values of ℓ and the extent of the region over which a significant variation of the local stiffness takes place. That is to say, the wider this region, the stronger the effect of the modulation on the amplitude of the backscattered wave, the extreme case being that considered in Figure 4 for $P_{\text{tip}} = 5$ MPa.

The investigation carried out on a surface-breaking crack was repeated with a subsurface crack. Contrary to the former case, the investigation on the latter yielded results which do not substantially differ from each other. For this reason, only the predictions on the dependence of the ratio R on the size of a crack, $d = (b - a)$, which is subjected to a pressure field decaying with a constant $\ell = 1$ mm are presented in Figure 7, those on the left being obtained for $P_{\text{tip}} = 5$ MPa, while those on the right refer to $P_{\text{tip}} = 70$ MPa. Each figure illustrates the behavior of R for three values of the ligament size: $a/\lambda_T = 0.4$, 1 and 2. The most relevant feature of these results is that, with the exception of a small range of values of $k_T d$

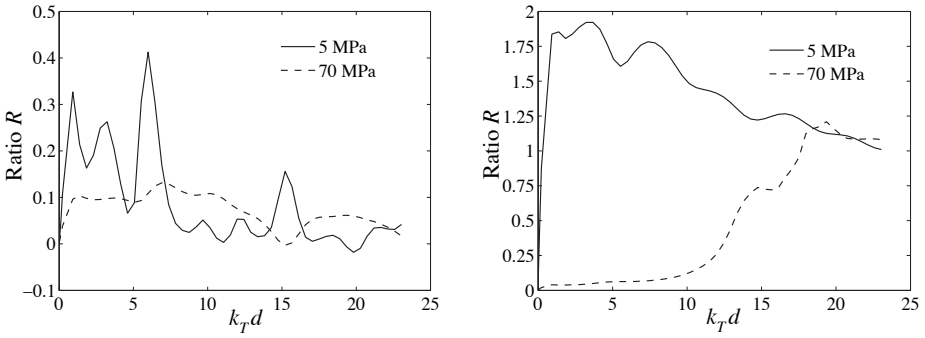

Figure 5. Ratio R versus nondimensional crack size $k_T d$ for values of the pressure at the crack tip equal to 5 MPa and 70 MPa. The pressure distribution decays exponentially from the crack tip with a characteristic length $\ell = 1$ mm. Left: dry surface-breaking crack. Right: water-confining surface-breaking crack.

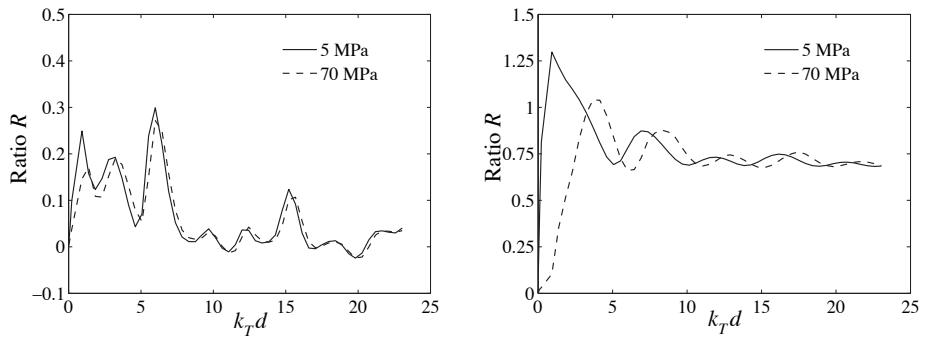

Figure 6. Ratio R versus nondimensional crack size $k_T d$ for values of the pressure at the crack tip equal to 5 MPa and 70 MPa. The pressure distribution decays exponentially from the crack tip with a characteristic length $\ell = 0.1$ mm. Left: dry surface-breaking crack. Right: water-confining surface-breaking crack.

corresponding to cracks smaller than one wavelength of the incident wave, the ratio R always remains below a threshold value of 0.3.

In view of earlier results proving the higher sensitivity of shear waves to small surface breaking cracks when they are insonified at angles of incidence just above the critical angle of longitudinal waves [Pecorari and Poznic 2005; Pecorari 2005], the behavior of the ratio R has been examined also under these conditions, and found to yield no clear criterion to discern subsurface from surface-breaking cracks.

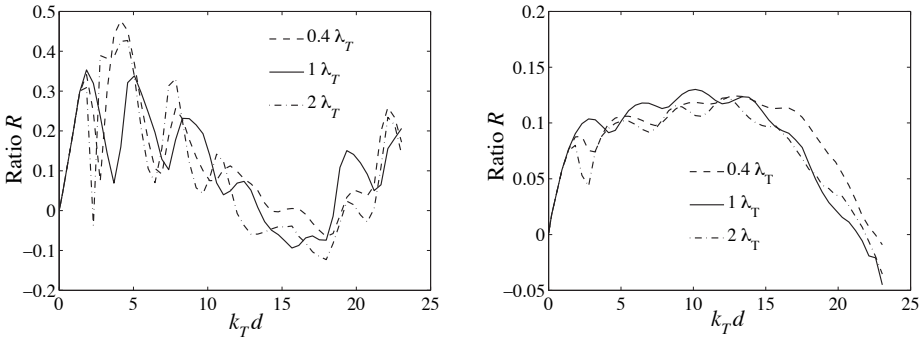

Figure 7. Ratio R versus nondimensional crack size $k_T d = k_T(b-a)$ for values of the ligament, a, equal to $0.4\lambda_T$, $1\lambda_T$, and $2\lambda_T$. The pressure distribution decays exponentially from the crack tip with a characteristic length $\ell = 1$ mm. Left: $P_{\text{tip}} = 5$ MPa. Right: $P_{\text{tip}} = 70$ MPa.

Similar negative results have obtained with longitudinal waves at 45 degrees, 60 degrees and 85 degrees incidence.

Finally, the results in Figure 8 concern the sensitivity of the ratio R to a variation of the angle on incidence from 45 degrees to 40 degrees, both for a surface-breaking crack filled with water (left), and for a dry subsurface crack (right). The pressure closing the crack is characterized by $P_{\text{tip}} = 70$ MPa and $\ell = 0.1$ mm, which is the less favorable of the two cases. Similar results have been obtained for an angle of incidence equal to 50 degrees and by reducing the value of the pressure at the crack tip to 5 MPa. The main conclusion to be drawn from the latter results is that the proposed technique appears to be robust within a variation of the angle of incidence of at least ± 5 degrees, since they confirm the results presented earlier.

5. Summary and concluding remarks

The potential use of the modulation technique to discern surface-breaking from subsurface cracks in components carrying pressurized water has been investigated theoretically. To that end, a model predicting the backscattered signal from dry and water-confining surface-breaking cracks and from subsurface cracks has been developed.

By using the backscattered signals recorded at the two turning points of a modulation cycle, $B^{-,+}$, and when the no modulation is applied, B_0, the ratio

$$R = \frac{B^- - B^+}{B_0}$$

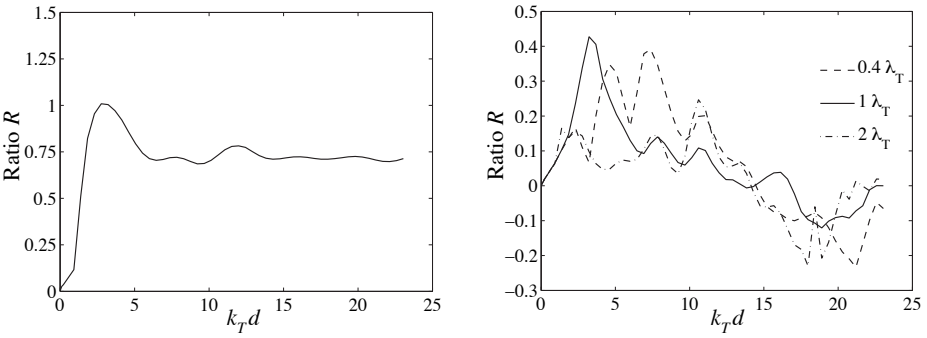

Figure 8. Ratio R versus nondimensional crack size $k_T d = k_T(b-a)$. The pressure distribution decays exponentially from the crack tip with a characteristic length $\ell = 0.1$ mm, and $P_{\text{tip}} = 70$ MPa. The angle of incidence is $\theta_{\text{in}} = 40$ degree. Left: Water-confining, surface-breaking crack. Right: subsurface crack with ligament size a equal to $0.4\lambda_T$, $1\lambda_T$, and $2\lambda_T$.

has been constructed. This ratio does not depend on the amplitude of the incident wave, though it appears to vary with both angle of incidence and wave polarization. For a shear vertical wave at 45 degree incidence, R is predicted to exceeds a threshold limit of 0.5 when a surface-breaking crack is filled with water, while it is always lower than 0.5 if the crack, whether surface-breaking or subsurface, is dry. The difference in the values of the ratio is ascribed to the dramatic variation of the normal stiffness of a partially closed, water-confining crack as the surfaces of the latter come into contact, and it may be used as a criterion for differentiating water-confining surface-breaking from subsurface cracks.

To confirm the validity of the proposed method a deeper investigation into the role of the rms roughness of the composite interface formed by the crack surfaces needs to be carried out. In fact, as illustrated in [Pecorari and Poznic 2005], the variation of the normalized normal stiffness of a water-confining interface is considerably reduced when the rms roughness of the interface increases from 0.1 μm to 1.5 μm. In this context, results by Parisi et al. [2000] (see also references therein) concerning the self-affine nature of the surfaces of fatigue cracks also need be taken into account if the profile of a stress-corrosion crack displays similar properties. Should this be the case, in fact, the extent to which a self-affine profile can be represented by models describing the statistical properties of an infinite interface treated as a stochastic process with spectrum containing components with arbitrarily small wavelengths must be reassessed. Of relevance to the behavior of the partially closed crack tip and to the model used to predict its acoustic response is

also the asymptotic behavior of the normal stiffness in proximity of the crack tip. In this work, the crack is assumed to be either uniformly closed or increasingly open as the observation point moves from the tip toward the mouth or center of the crack. Watanabe et al. [2005] have recently brought to the authors' attention the incompatibility between the asymptotic behavior of the stress ($\propto \sqrt{1/r}$) and of the displacement discontinuity ($\propto \sqrt{r}$) when the crack stiffness is assumed to be constant and finite. This incompatibility would be removed if the self-affine nature of the crack surfaces were considered. In fact, the rms roughness evaluated over an interval shorter than the smaller cut-off wavelength of the profile's power spectrum, and including the crack tip, would be zero. Thus, the crack would be either completely open or completely closed in the neighborhood of its crack tip. In the first case $K_N = 0$, in the second $K_N \to \infty$, and in both the use of the spring boundary conditions would be compatible with the assumed asymptotic behavior of the quantities involved. However, whether either condition would extend far enough from the crack tip to affect the numerical solution of the scattering problem obtained in this work remains a matter to investigate. The limits of the model notwithstanding, it is the authors' opinion that the proposed method deserves the consideration of a working hypothesis for further experimental investigation, and that alone can provide a definite answer to the problem of interest to this communication.

Acknowledgments

This work was carried out as part of the project entitled "Detection of stress-corrosion cracks by means of nonlinear scattering of ultrasonic waves" which is sponsored by the Swedish Centre for Nuclear Technology.

Appendix

In this appendix, the integral equations and the formulas expressing the displacement components of the scattered field in terms of the solutions of the former are given in the case in which the crack is subsurface. The integral equations are found by enforcing the boundary conditions given in equations (3–1) and (3–2) on the general solutions of the equations of motion. These equations are singular and decoupled. Their unknowns, $A(S)$ and $B(S)$, are functions representing the tangents of the tangential and normal crack opening displacement components, respectively.

Let A_{in} be the amplitude of the incident wave and ξ the transform variable used in the integral representation of the general solution of the equations of motion

(3–4)–(3–7). Introduce the normalized quantities and coordinates

$$\bar{A} = A_{\text{in}} k_L,\ \bar{a} = a k_L,\ \bar{b} = b k_L,\ X = x k_L,\ Y = y k_L,$$
$$\zeta = k_L \xi,\ \beta_L = k_L \alpha_L,\ \text{and } \beta_T = k_L \alpha_T,$$

in which k_L is the wave number of the incident wave; also let H be the Heaviside unit step function. The integral equation for the symmetric problem then becomes

$$\int_{\bar{a}}^{\bar{b}} B(S)\left(\frac{1}{S+Y} - \frac{2\pi\kappa^2}{1-\kappa^2}\bar{K}_N(Y)H(S-Y) + \frac{1}{1-\kappa^2}\int_0^\infty (I_1+I_2)\,d\zeta\right) dS + \int_{\bar{a}}^{\bar{b}} \frac{B(S)}{S-Y}\,dS = \frac{\pi\kappa^2}{2(\kappa^2-1)}\frac{\bar{\sigma}^I_{xx}(Y)}{\bar{A}}, \quad \text{(A-1)}$$

where

$$I_1 = \int_0^\infty \frac{(\kappa^2+2\beta_L^2)(\beta_T^2+\zeta^2)e^{-\beta_L Y} - 4\beta_L\beta_T\zeta^2 e^{-\beta_T Y}}{4\zeta^2\beta_L\beta_T - (\zeta^2+\beta_T^2)^2}\left(F_1 e^{\beta_L S} + F_2 e^{\beta_T S}\right) d\zeta,$$

$$I_2 = \int_0^\infty \left(\frac{(\zeta^2+\beta_T^2)^2 - 4\zeta^2\beta_L\beta_T}{\zeta\beta_L} - \left(2-2\kappa^2\right)\right)\sin(\zeta S)\cos(\zeta Y)\,d\zeta,$$

with $F_1 = \left(-\kappa^2(2-\kappa^2) - 4\beta_L^2\zeta^2\right)/\beta_L^2$ and $F_2 = 4\zeta^2$.

The integral equation associated with the antisymmetric problem is

$$\int_{\bar{a}}^{\bar{b}} B(S)\left(\frac{1}{S+Y} + \frac{\pi\kappa^2}{\kappa^2-1}\bar{K}_T(Y)H(S-Y) + \frac{4}{\kappa^2-1}\int_0^\infty (I_3+I_4)\,d\zeta\right) dS + \int_{\bar{a}}^{\bar{b}} \frac{A(S)}{S-Y}\,dS = \frac{\pi}{(1-\kappa^2)}\frac{\bar{\tau}^I_{xy}(Y)}{\bar{A}}, \quad \text{(A-2)}$$

where

$$I_3 = \int_0^\infty \frac{-4\zeta^2\beta_L\beta_T e^{-\beta_L Y} + (2\zeta^2+\kappa^2)^2 e^{-\beta_T Y}}{4\zeta^2\beta_L\beta_T - (\beta_T^2+\zeta^2)^2}\left(E_1 e^{-\beta_L S} + E_2 e^{-\beta_T S}\right) d\zeta,$$

$$I_4 = \int_0^\infty \left(\frac{4\zeta^2\beta_L\beta_T - (\zeta^2+\beta_T^2)^2}{4\zeta\beta_T} - \tfrac{1}{2}\left(\kappa^2-1\right)\right)\sin(\zeta S)\cos(\zeta Y)\,d\zeta,$$

with $E_1 = -\zeta^2$ and $E_2 = (\zeta^4 - \zeta^2\kappa^2 + \kappa^2/4)/\beta_T^2$. If the crack is surface-breaking, additional terms appear in the integrals I_1 and I_3, namely $F_3 = \kappa^2(2-\kappa^2)/\beta_L^2$ and $E_3 = -\kappa^4/4\beta_T^2$, respectively; see also [Mendelsohn et al. 1980]. In all these expressions $\kappa = k_T/k_L$. The right-hand sides of (A-1) and (A-2) are the respective components of the stress field carried by the incident wave.

The components of the displacement field scattered by a subsurface crack, normalized by the amplitude of the incident wave A_{in} and propagating in the positive quarter-space, are given by the following expression:

Symmetric problem.

$$U^S(X,Y) = \frac{2}{\pi}\int_0^\infty d\zeta \int_{\bar a}^{\bar b} \left(\frac{(\beta_T^2+\zeta^2)(F_1 e^{-\beta_L S}+F_2 e^{-\beta_T S})}{\kappa^2\left(4\zeta^2\beta_L\beta_T-(\beta_T^2+\zeta^2)^2\right)} \left(\zeta e^{-\beta_L Y} - \frac{2\zeta\beta_L\beta_T}{\beta_T^2+\zeta^2} e^{-\beta_T Y}\right) \sin(\zeta X) + \left(\frac{2\zeta}{\kappa^2} e^{-\beta_T X} - \frac{\beta_T^2+\zeta^2}{\zeta\kappa^2} e^{-\beta_L X}\right) \cos(\zeta Y)\sin(\zeta S)\right) B(S)\,dS,$$

$$V^S(X,Y) = \frac{2}{\pi}\int_0^\infty d\zeta \int_{\bar a}^{\bar b} \left(\frac{(\beta_T^2+\zeta^2)(F_1 e^{-\beta_L S}+F_2 e^{-\beta_T S})}{\kappa^2\left(4\zeta^2\beta_L\beta_T-(\beta_T^2+\zeta^2)^2\right)} \left(\beta_L e^{-\beta_L Y} - \frac{2\zeta^2\beta_L}{\beta_T^2+\zeta^2} e^{-\beta_T Y}\right) \cos(\zeta X) + \left(\frac{2\beta_T}{\kappa^2} e^{-\beta_T X} - \frac{(\beta_T^2+\zeta^2)}{\beta_L\kappa^2} e^{-\beta_L X}\right) \sin(\zeta Y)\sin(\zeta S)\right) B(S)\,dS.$$

Antisymmetric problem.

$$U^a(X,Y) = \frac{2}{\pi}\int_0^\infty d\zeta \int_{\bar a}^{\bar b} \left(\frac{(E_1 e^{-\beta_L S}+E_2 e^{-\beta_T S})}{4\zeta^2\beta_L\beta_T-(\beta_T^2+\zeta^2)^2} \left(4\zeta^2\beta_T e^{-\beta_L Y} - 2\beta_T(\beta_T^2+\zeta^2) e^{-\beta_T Y}\right) \cos(\zeta X) - \left(\beta_L e^{-\beta_L X} - \frac{\beta_T^2+\zeta^2}{2\beta_T} e^{-\beta_T X}\right) \sin(\zeta Y)\sin(\zeta S)\right) A(S)\,dS,$$

$$V^a(X,Y) = \frac{2}{\pi}\int_0^\infty d\zeta \int_{\bar a}^{\bar b} \left(\frac{(E_1 e^{-\beta_L S}+E_2 e^{-\beta_T S})}{4\zeta^2\beta_L\beta_T-(\beta_T^2+\zeta^2)^2} \left(-4\zeta\beta_T\beta_L e^{-\beta_L Y} + 2\zeta(\beta_T^2+\zeta^2) e^{-\beta_T Y}\right) \sin(\zeta X) - \left(\zeta e^{-\beta_L X} - \frac{\beta_T^2+\zeta^2}{2\zeta} e^{-\beta_T X}\right) \cos(\zeta Y)\sin(\zeta S)\right) A(S)\,dS.$$

Similar expressions for the displacement components scattered by a surface-breaking crack can be found in [Mendelsohn et al. 1980].

References

[Achenbach et al. 1980] J. D. Achenbach, L. M. Keer, and D. A. Mendelsohn, "Elastodynamic analysis of an edge crack", *J. Appl. Mech.* (*Trans. ASME*) **47**:3 (1980), 551–556. MR 81j:73073

[Baik and Thompson 1984] J. M. Baik and R. B. Thompson, "Ultrasonic scattering from imperfect interfaces: a quasi-static model", *J. Nondestr. Eval.* **4**:3–4 (1984), 177–196.

[Baltazar et al. 2002] A. Baltazar, S. I. Rokhlin, and C. Pecorari, "On the relationship between ultrasonic and micromechanical properties of contacting rough surfaces", *J. Mech. Phys. Solids* **50**:7 (2002), 1397–1416.

[Brind and Achenbach 1981] R. J. Brind and J. D. Achenbach, "Scattering of longitudinal and transverse waves by a sub-surface crack", *J. Sound Vib.* **78** (1981), 555–563.

[Chan and Horn 1985] D. Y. C. Chan and R. G. Horn, "The drainage of thin liquid films between solid surfaces", *J. Chem. Phys.* **83**:10 (1985), 5311–5324.

[Das et al. 1996] S. K. Das, M. M. Sharma, and R. S. Schechter, "Solvation force in confined molecular fluids using molecular dynamics simulation", *J. Phys. Chem.* **100**:17 (1996), 7122–7129.

[Drinkwater et al. 1996] B. W. Drinkwater, R. S. Dwyer-Joyce, and P. Cawley, "A study of the interaction between ultrasound and a partially contacting solid-solid interface", *P. Roy. Soc. Lond. A Mat.* **452**:1955 (1996), 2613–2628.

[Grabbe and Horn 1993] A. Grabbe and R. G. Horn, "Double-layer and hydration forces measured between silica sheets subjected to various surface treatments", *J. Colloid Interf. Sci.* **157**:2 (1993), 375–383.

[Ho et al. 1998] R. Ho, J. Y. Yuan, and Z. Shao, "Hydration force in the atomic force microscope: a computational study", *Biophys. J.* **75**:2 (1998), 1076–1083.

[Israelachvili 1992] J. N. Israelachvili, *Intermolecular and surface forces*, 2nd ed., Academic Press, London, 1992.

[Jenssen et al. 2000] A. Jenssen, K. Norrgård, R. Lundström, B. Claesson, and H. Ericsson, "Metallographic examination of cracks in nozzle to safe-end weld of alloy 182 in Ringhals 4", Technical Report N(H)-00/099, Studsvik, 2000.

[Kazakov et al. 2002] V. V. Kazakov, A. Sutin, and P. A. Johnson, "Sensitive imaging of an elastic nonlinear wave-scattering source in a solid", *Appl. Phys. Lett.* **81**:4 (2002), 646–648.

[Kim et al. 2004a] J. Y. Kim, A. Baltazar, and S. I. Rokhlin, "Ultrasonic assessment of rough surface contact between solids from elastoplastic loading-unloading hysteresis cycle", *J. Mech. Phys. Solids* **52**:8 (2004), 1911–1934.

[Kim et al. 2004b] J. Y. Kim, V. A. Yakovlev, and S. I. Rokhlin, "Surface acoustic wave modulation on a partially closed fatigue crack", *J. Acoust. Soc. Am.* **115**:5 (2004), 1961–1972.

[Lavrentyev and Rokhlin 1998] A. I. Lavrentyev and S. I. Rokhlin, "Ultrasonic spectroscopy of imperfect contact interfaces between a layer and two solids", *J. Acoust. Soc. Am.* **103**:2 (1998), 657–664.

[Mendelsohn et al. 1980] D. A. Mendelsohn, J. D. Achenbach, and L. M. Keer, "Scattering of elastic waves by a surface-breaking crack", *Wave Motion* **2**:3 (1980), 277–292.

[Nagy 1992] P. B. Nagy, "Ultrasonic classification of imperfect interfaces", *J. Nondestr. Eval.* **11**:3–4 (1992), 127–140.

[Newman et al. 2003] J. A. Newman, W. T. Riddell, and R. S. Piascik, "Analytical and experimental study of near-threshold interactions between crack closure mechanisms", Technical report TM-2003-211755, ARL-TR-2774, NASA, 2003, Available at http://citeseer.ist.psu.edu/615746.html.

[Parisi et al. 2000] A. Parisi, G. Caldarelli, and L. Pietronero, "Roughness of fracture surfaces", *Europhys. Lett.* **52**:3 (2000), 304–310.

[Pashley and Israelachvili 1984] R. M. Pashley and J. N. Israelachvili, "Molecular layering of water in thin films between mica surfaces and its relation to hydration forces", *J. Colloid Interf. Sci.* **101**:2 (1984), 511–523.

[Pecorari 2005] C. Pecorari, "A note on the sensitivity of *SV* wave scattering to surface-breaking cracks", *Ultrasonics* **43**:7 (2005), 508–511.

[Pecorari and Poznic 2005] C. Pecorari and M. Poznic, "Nonlinear acoustic scattering by a partially closed surface-breaking crack", *J. Acoust. Soc. Am.* **117**:2 (2005), 592–600.

[Pecorari and Poznic 2006] C. Pecorari and M. Poznic, "On the linear and nonlinear acoustic properties of dry and water-confining elasto-plastic interfaces", *P. Roy. Soc. Lond. A Mat.* **462**:2067 (2006), 769–788.

[Rokhlin et al. 2004] S. I. Rokhlin, L. Wang, B. Xie, V. A. Yakovlev, and L. Adler, "Modulated angle beam ultrasonic spectroscopy for evaluation of imperfect interfaces and adhesive bonds", *Ultrasonics* **42**:1–9 (2004), 1037–1047.

[Watanabe et al. 2005] K. Watanabe, S. Ueda, and S. Biwa, 2005. private communication.

[Xiao and Nagy 1998] H. Xiao and P. B. Nagy, "Enhanced ultrasonic detection of fatigue cracks by laser-induced crack closure", *J. Appl. Phys.* **83**:12 (1998), 7453–7460.

Received 15 Dec 2005.

MILAN POZNIC: milan@kth.se
Marcus Wallenberg Laboratory, Department of Aeronautical and Vehicle Engineering, Royal Institute of Technology, SE 10044 Stockholm, Sweden

CLAUDIO PECORARI: pecorari@kth.se
Marcus Wallenberg Laboratory, Department of Aeronautical and Vehicle Engineering, Royal Institute of Technology, SE 10044 Stockholm, Sweden